Journal of Power Sources 556 (2023) 232516

Contents lists available at ScienceDirect

Journal of Power Sources

journal homepage: www.elsevier.com/locate/jpowsour

High thermoelectric performance of spray-coated Poly (3,4-ethylenedioxythiophene):poly(styrenesulfonate) films enabled by two-step post-treatment process

Yen-Ting Lin [a], Chia-Yu Lee [a], Chih-Yao Wu [b], Jhih-Min Lin [c], Tai-Chou Lee [b], Shih-Huang Tung [d], Cheng-Liang Liu [a,*]

[a] Department of Materials Science and Engineering, National Taiwan University, Taipei, 10617, Taiwan
[b] Department of Chemical and Materials Engineering, National Central University, Taoyuan, 32001, Taiwan
[c] National Synchrotron Radiation Research Center, Hsinchu, 30076, Taiwan
[d] Institute of Polymer Science and Engineering, National Taiwan University, Taipei, 10617, Taiwan

HIGHLIGHTS

- Spray-coated PEDOT:PSS films for thermoelectric application.
- Enhanced thermoelectric properties by two-step pretreatment process.
- A flexible 14-leg thermoelectric module generates thermopower from low-grade heat.

GRAPHICAL ABSTRACT

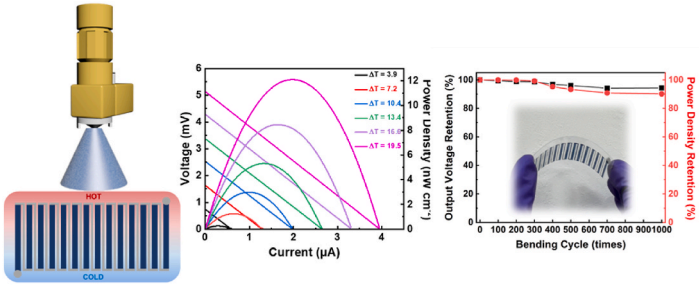

ARTICLE INFO

Keywords:
Thermoelectric
PEDOT:PSS
Spray-coating
Doping
Thermoelectric generator

ABSTRACT

Herein, poly (3,4-ethylenedioxythiophene):poly (styrenesulfonate) (PEDOT:PSS) films with improved thermoelectric properties are fabricated via spray coating followed by a sequential, two-step post-treatment process with ethylene glycol (EG) and a methylammonium iodide (MAI) solution. The EG treatment greatly increases the electrical conductivity of the PEDOT-PSS film up to 1752.1 S cm^{-1}, with an unchanged Seebeck coefficient of 15–17 μV K^{-1}, while the optimal use of 0.05 M MAI in DMSO/DI water for the second step provides a high power factor of 122.3 μW m^{-1} K^{-2}, along with an increased conductivity of 2226.8 S cm^{-1} and Seebeck coefficient of 22.8 μV K^{-1}. Notably, the obtained power factor is among the highest reported for spray-coated polymer-based thermoelectric devices. The performance enhancement is attributed to phase separation of the non-conductive PSS from the PEDOT, the change in chain conformation, the preferential orientation of the PEDOT crystallites, and the manipulation of energy levels. High thermoelectric performance of the as-fabricated PEDOT:PSS on a plastic substrate is established by using a facile proof-of-concept thermoelectric generator to generate a maximum power density of 12.1 nW cm^{-2}. The fabrication approach developed herein provides an essential paradigm for the production of polymer thermoelectric materials with great potential for application in wearable thermoelectric devices.

* Corresponding author.
E-mail address: liucl@ntu.edu.tw (C.-L. Liu).

https://doi.org/10.1016/j.jpowsour.2022.232516
Received 9 October 2022; Received in revised form 2 December 2022; Accepted 8 December 2022
Available online 15 December 2022

1. Introduction

Poly (3,4-ethylenedioxythiophene):poly (styrenesulfonate) (PEDOT:PSS) has recently emerged as the benchmark conducting polymer material for thermoelectric energy harvesting, due to its high electrical conductivity, low intrinsic thermal conductivity, good environmental stability, and commercial availability [1–10]. An efficient organic thermoelectric material with a high power factor (PF) requires a high electrical conductivity (σ) and Seebeck coefficient (S), as the PF is given by σS^2. Hence, the modification of the PEDOT:PSS film via pre-doping or post-treatment processes in order to achieve a large PF via adjustable electrical conductivity and thermopower capability would be expected to provide a high conversion efficiency [11–14]. However, the simultaneous optimization of the electrical conductivity and Seebeck coefficient is inherently challenging because these two performance parameters are mutually interdependent [15–20]. In this respect, post-treatment of the PEDOT:PSS with secondary dopants can be used to induce changes in the microstructure and molecular orientation [21–26], thereby efficiently improving the electrical conductivity while not decreasing, or even slightly increasing the Seebeck coefficient. In particular, polar organic solvents are widely used as secondary dopants, such as ethylene glycol (EG) [27,28], dimethyl sulfoxide (DMSO) [27,29], ethanolamine/ammonia solution [30] and methanol/ethanol solution [31]. The screening effect from high dielectric polar solvent can triple the electrical conductivity with a nearly unchanged Seebeck coefficient. Compared with the use of neat organic solvents, the post-treatment with organic salt (methylammonium iodide, MAI) and polar solvent/water cosolvents yields an optimal power factor of 144 $\mu W\ m^{-1}\ K^{-2}$ [32] with enhancing both electrical conductivity and Seebeck coefficient for the PEDOT:PSS film. Further, the synergetic effects of a two-step post-treatment with secondary dopants can provide PEDOT:PSS films with even more significant enhancements in thermoelectric performance [33–40].

Despite the considerable increase in the power factor of PEDOT:PSS films over the last decade, solution-based coating/printing techniques are important for providing a versatile solution to the manufacture of PEDOT:PSS materials with improved thermoelectric efficiency via controlled ink formulation and film microstructure [41]. Therefore, the processing-structure-property relationships of the fabricated thermoelectric materials and devices need to be established to enable the coating of nanoscale components and macroscopic energy devices. Although spin coating and drop casting are the most extensively used methods for PEDOT:PSS film deposition, these face difficulties with respect to large area coverage and batch operation. By contrast, spray-coating is a large-scale, high throughput process that is highly suited to the fabrication of such coatings onto substrates of any shape and geometry with low material consumption and good industrial scalability [42–45]. Additionally, a desired polymer thermoelectric film pattern can be ensured by employing a shadow mask during spraying. However, in order to realize the spray-coating/printing of thermoelectric devices with competitive performances, an accessible post-treatment process must be developed for the PEDOT:PSS films.

Herein, the thermoelectric characteristics of spray-coated PEDOT:PSS films are reported following a two-step post-treatment process aimed at simultaneously enhancing the electrical conductivity and Seebeck coefficient. The results indicate that the selection of EG as the solvent for the first post-treatment step, and optimization of the MAI salt solution concentration for the second step, provides the best power factor of 122.3 $\mu W\ m^{-1}\ K^{-2}$. The effective PSS removal and the optimum doping level of the PEDOT:PSS film are verified by X-ray photoelectron spectroscopy (XPS) and absorption spectroscopy, and the thermoelectric mechanism is further elucidated by Raman spectroscopy and ultraviolet photoelectron spectroscopy (UPS). In addition, the crystalline film morphologies are examined by atomic force microscopy (AFM), and their crystallinity and orientations are detected by two-dimensional grazing-incidence wide-angle X-ray scattering (2D GIWAXS). Finally, a flexible p-type thermoelectric generator comprising fourteen spray-printed PEDOT:PSS legs is shown to produce an output power density of 12.1 $nW\ cm^{-2}$ at a low temperature gradient of 19.5 K.

2. Results and discussion

2.1. Thermoelectric film fabrication

The fabrication procedure for the various PEDOT:PSS/MAI thermoelectric composite film is shown schematically in Fig. 1, and the fabrication and post-treatment conditions that were employed to obtain samples A–E are listed in Table 1. For sample A, a PEDOT:PSS solution was directly sprayed onto the preheated glass substrate, followed by thermal annealing. The PEDOT:PSS film quality was controlled and optimized by the viscosity and flow rate of the spraying solution, the solvent used, air pressure, the distance between nozzle and substrate, etc, as described in experimental section. For sample B, the post-treatment involved the use of EG organic solvent, while samples C, D, and E, were obtained via the two-step post-treatment with EG followed by various concentrations of MAI in DMSO/DI water cosolvent. The MAI salt solution is expected to result in phase separation of the PEDOT:PSS components, thereby resulting in the selective removal of the PSS. The MAI post-treatment significantly improves the power factor of the PEDOT:PSS film without a trade-off between the electrical conductivity and Seebeck coefficient, as demonstrated later.

2.2. X-ray photoemission spectroscopy (XPS)

The effects of both EG and MAI upon the oxidation levels of the PEDOT chains and, hence, the thermoelectric properties of the material, are revealed by the XPS results in Fig. 2. Here, the high-resolution S 2p spectra of samples A–E clearly distinguish the signals due to the PSS sulfonate groups at 166–172 eV and the PEDOT thiophene units at 162–166 eV due to the different chemical environments of their sulfur atoms (Fig. 2a–e). Further, as shown in Fig. 2f, the ratio of PSS to PEDOT decreases significantly, from 2.42 for sample A to 2.11 for sample B, due to the EG post-treatment step, and is further reduced to 1.32, 1.13, and 1.49 with increasing MAI concentration in the second step for samples C, D, and E respectively. The XPS results indicate that sample D has a significantly increased PEDOT content compared to that of the pristine PEDOT:PSS film (sample A), with 51.2% of the PSS chains being removed via the optimal two-step post-treatment. This is attributed to the high dielectric constant of the EG, which shields the coulombic interactions between the PEDOT and PSS, followed by further phase separation of these chains due to the diffusion of MA^+ ions from MAI during the second post-treatment step. This selective removal of nonconductive PSS over PEDOT may allow for faster charge transport across the conducting channels.

2.3. Morphology analysis

The morphological changes in the various PEDOT:PSS films due to the selective removal of PSS are revealed by the AFM images in Fig. 3. Here, small, bright spherical domains are prevalent on the surface of sample A due to the PEDOT-rich phases, and are separated by dark regions representing the insulating PSS domains [46,47] (Fig. 3a). Further, the post-treatments with EG and MAI are seen to result in an increase in the fraction of high-contrast PEDOT spherical domains, with sample D having the highest fraction. This is accompanied by a corresponding increase in the quantitative root-mean-square roughness (R_{rms}) from 1.47 nm for sample A to 1.69, 1.77, 1.95, and 1.99, and 1.95 for samples C, B, E, and D, respectively. These results can be attributed to the more selective removal of the over-doped PSS chains from sample D, which may be expected to generate an effective charge transport pathway for the hopping process. Meanwhile, the surface morphologies of sample A-E are also characterized by SEM, as shown Fig. S1. The smooth surface

morphologies of PEDOT:PSS films under various post-treatment conditions have been observed, representing good reliability of the spray-coating process for polymer films.

2.4. Molecular orientation

The structural ordering of the PEDOT:PSS films before and after the post-treatment process are indicated by the GIWAXS results in Fig. 4, where the scattering rings located at q_{xy} ~1.2 and 1.8 Å^{-1} are characteristic of the PSS and PEDOT aggregates, respectively. For sample A, the diffuse scattering profile indicates a lack of ordering in the film (Fig. 4a), whereas samples B–E exhibit higher-order PEDOT lamellar scattering in the out-of-plane direction (along q_z) with an interlayer distance of 0.27 Å (Fig. 4b–e). Moreover, the scattering ring due to the π-π stacking of the PEDOT chains of each post-treated film at q_{xy} ~1.8 Å^{-1} is seen to intensify relative to the scattering due to the PSS at q_{xy} ~1.2 Å^{-1}, especially along the q_{xy} direction. This reflects the increased fraction of PEDOT, which prefers to arrange in an edge-on orientation, with the aromatic backbones being oriented perpendicularly to the substrate surface, and the π-stacking plane oriented along the surface. Among the various films, sample D exhibits the most oriented PEDOT stacking, thereby confirming the correlation between the degree of ion exchange and the structural transformation of the post-treated PEDOT:PSS films suggested by the above AFM results.

2.5. Spectroscopic properties

The confirmational changes of the PEDOT:PSS chains are further demonstrated by the Raman spectra in Fig. 5a, where each sample exhibits characteristic peaks and regions corresponding to the PEDOT and PSS bond stretching and bending vibrations. In detail, the strongest bands in the range of 1400–1500 cm^{-1} correspond to the $C_\alpha = C_\beta$ symmetric stretching of the PEDOT thiophene rings, while the vibrational modes at 1257 and 1580 cm^{-1} correspond to the PSS stretching vibration. Notably, a distinct redshift is observed in the PEDOT vibrational peak from 1435 cm^{-1} for sample A to ~1430 cm^{-1} in sample D due to the DMSO and MAI secondary dopants (Fig. 5b). This indicates the structural change from the coiled benzoid to the more planar/linear quinoid in the PEDOT resonance, as demonstrated by the schematic illustration in Fig. S2 of the Supplementary Material. This structural change allows for better PEDOT packing, and usually denotes more efficient charge delocalization.

Table 1
The fabrication procedure for all PEDOT:PSS-based thermoelectric films (sample A-E) and their corresponding thermoelectric properties.

Sample	1st post-treatment	2nd post-treatment	S (μV K^{-1})	σ (S cm^{-1})	PF (μW m^{-1} K^{-2})
sample A	–	–	16.7	6.1	0.2
sample B	EG	–	17.9	1752.1	56.6
sample C	EG	0.01 M MAI in DMSO/DI water	18.9	1016.4	36.5
sample D	EG	0.05 M MAI in DMSO/DI water	22.8	2226.8	122.3
sample E	EG	0.1 M MAI in DMSO/DI water	21.3	1784.7	80.9

The effects of the two-step EG and MAI post-treatment processs upon the electronic structures of the PEDOT:PSS films are indicated by the UPS results in Fig. 6. The work functions of the samples are identified by measuring the cut-off energy of the secondary peak in the lower kinetic energy region (Fig. 6a). Here, sample A has a work function of 5.1 eV, which is in good agreement with the values reported in the literature [48–50], while samples B, C, E, and D exhibit decreasing values of 5.0, 4.9, 4.7, and 4.5 eV, respectively. The local structural distortion of PEDOT:PSS leads to localized positively charged defects (i.e. polarons), and a new in-gap state is formed according to the instability of the localized level from the top of the highest occupied molecular orbital (HOMO) [51], as shown in Fig. S3. The decreased work functions of the post-treatment samples enable a metallic network of polarons to be formed, with the Fermi level lying in the delocalized polaron band [23, 52–54], thereby promoting charge carrier transport capability. This also agrees with the UV–Vis spectra provided in Fig. S4, where the absorption band between 600 and 1000 nm refers to the polaron state of the

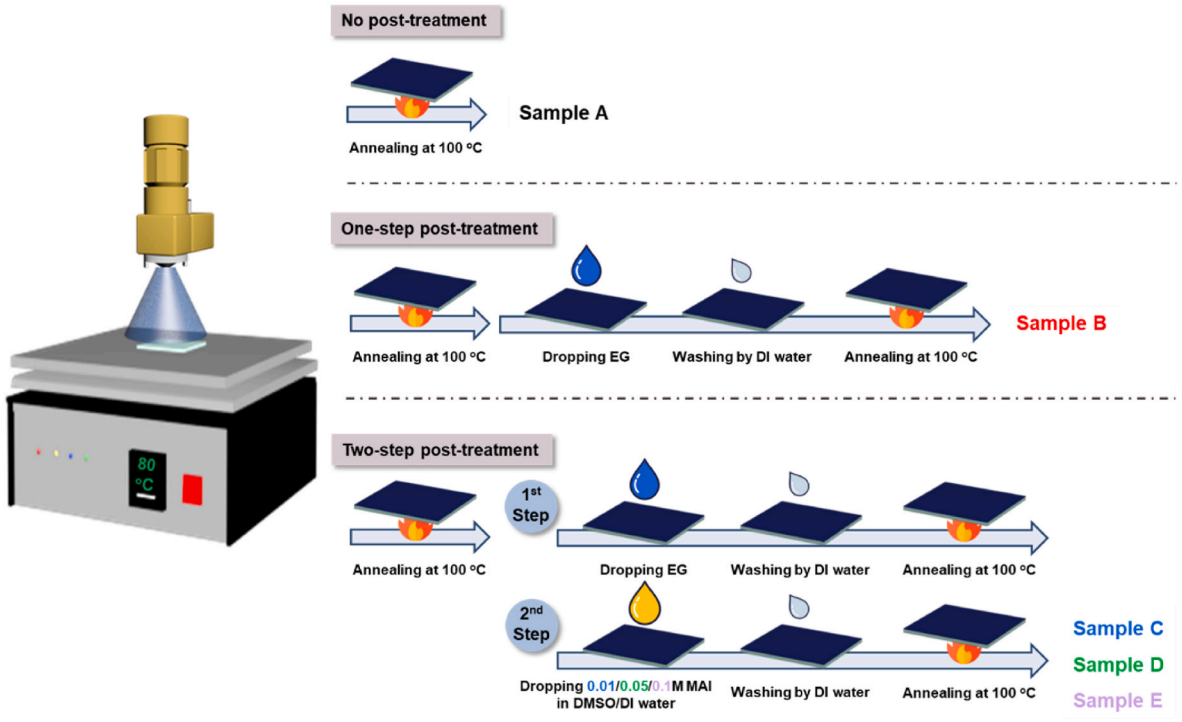

Fig. 1. Schematic of fabrication and sequential post-treatment of PEDOT:PSS film with EG and MAI in DMSO/deionized water (sample A-E).

post-treated PEDOT:PSS film. Likewise, Fig. 6a shows the lower binding energy region of the UPS, where the onset of the sharp increase in binding energy corresponds to the energy gap between the HOMO and the Fermi level. The work function, Fermi, and HOMO levels of all the samples are labeled in Fig. 6b. Thus, for sample D, the HOMO shifts away from the Fermi level by about 0.20 eV (from 0.52 to 0.72 eV) and the work function decreases to ~4.5 eV, corresponding to a shift of 0.6 eV relative to sample A. As Mott's formula indicates, the HOMO moves away from the Fermi level, which may account for the enlarged Seebeck coefficient [55,56]. Hence, the two-step post-treated samples are expected to exhibit enhancements in both their electrical conductivities and Seebeck coefficients due to their more ordered structures and polaron state compositions.

2.6. Thermoelectric properties

The spray-coated PEDOT:PSS films were prepared for thermoelectric characterization by painting Ag paste on both ends for contact pads, and the thermoelectric properties were characterized at a temperature of 323 K in an inert helium atmosphere. The Seebeck coefficients, electrical conductivities, and power factors of the PEDOT:PSS films are presented in Fig. 7. Due to the excessive presence of insulating PSS^- in the PEDOT:PSS solution, sample A exhibits poor thermoelectric properties, with a Seebeck coefficient of 16.7 μV K^{-1}, a conductivity of 6.1 S cm^{-1}, and a corresponding power factor only ~0.2 μW m^{-1} K^{-2} (Fig. 7a–c). By contrast, sample B exhibits a high conductivity of 1752.1 S cm^{-1}, a slightly increased Seebeck coefficient of 17.9 mV K^{-1}, and an increased power factor of ~56.6 μW K^{-2} m^{-1} due to the EG post-treatment step (Fig. 7a–c). Moreover, the observed conductivity and Seebeck coefficient are consistent with the previously reported values. Thus, the EG post-treatment step can significantly enhance the conductivity while maintaining the Seebeck coefficient by weakening the Coulombic interaction between $PEDOT^+$ and PSS^-. Moreover, due to the additional post-treatment step with MAI, the Seebeck coefficient further increases to 18.9 and 22.8 μV K^{-1} for samples C and D, respectively (Fig. 7a). The corresponding conductivities and power factors are 1016.1 S cm^{-1} and 36.5 μW K^{-2} m^{-1} for sample C, and 2226.8 S cm^{-1} and 122.3 μW K^{-2} m^{-1} for sample D. However, sample E exhibits a slight deterioration in both conductivity and Seebeck coefficient (1784.2 S cm^{-1} and 21.3 μV K^{-1} respectively) due to the higher concentration of MAI (Fig. 7a and b). Thus, sample D exhibits the optimal Seebeck coefficient, conductivity, and power factor due to the synergetic conformation change of the PEDOT chain, phase separation between PEDOT and PSS, and removal of PSS via the two-step post-treatment process. The observed power factor is compared to the existing experimental results from the spray-coated polymer-based thermoelectric films, as listed in Table S1, while the previously reported power factors, conductivities, and Seebeck coefficients are compared with those obtained herein for sample D in Fig. 7d and e. Here, the previously reported results indicate conductivities ranging from 70 to 600 S cm^{-1}, and Seebeck coefficients residing mainly in the range of 15–30 μV K^{-1} (with one extreme value of 93 μV K^{-1} for the inorganic Te–Bi_2Te_3 [57]), while the highest power factor of 60 μW m^{-1} K^{-2} is achieved by the spray-coated PEDOT:PSS/Te–Bi_2Te_3 hybrid. This clearly demonstrates that the observed Seebeck coefficient of sample D falls within the moderate-to-high region of the reported range, while a significant enhancement in electrical conductivity can be obtained. Factors impacting these results include the two-step sequential solvent and MAI post-treatment processes, which can promote the

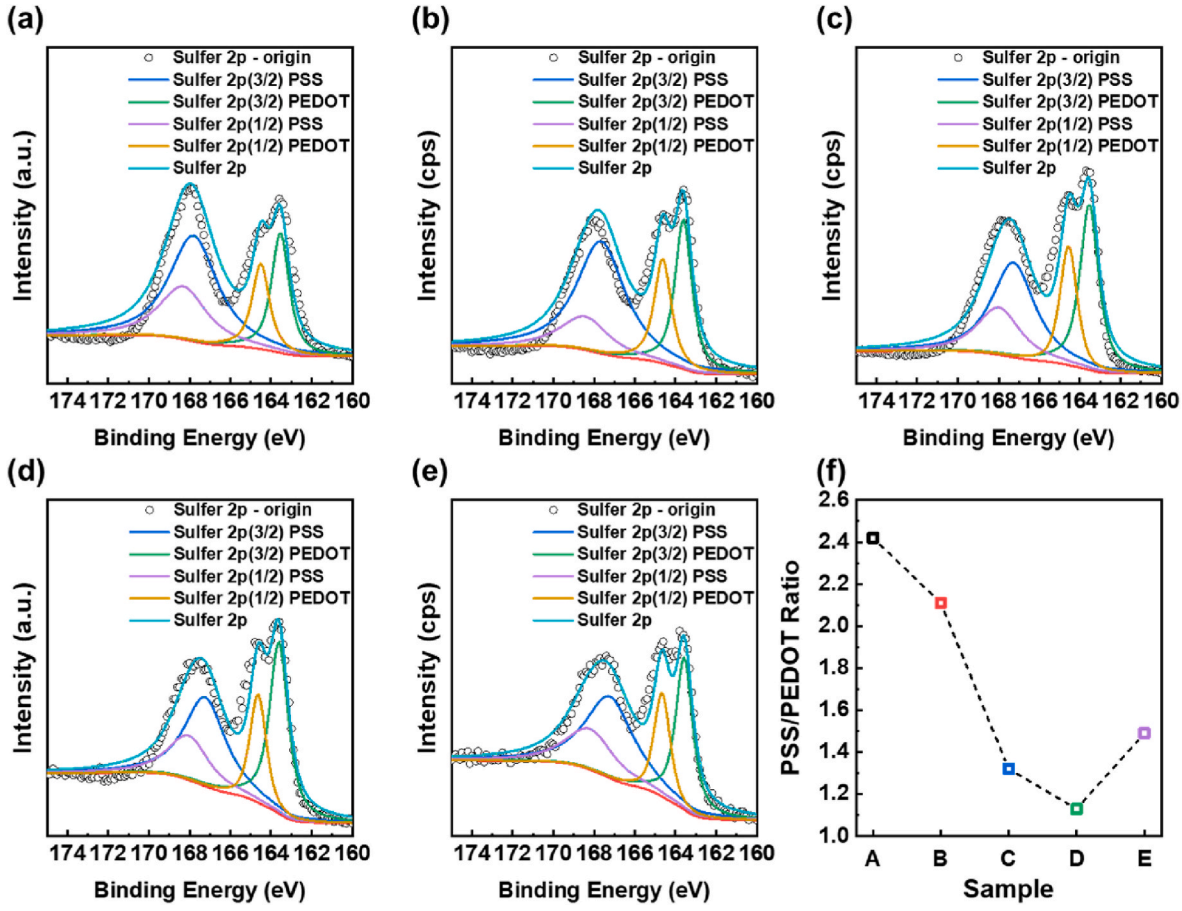

Fig. 2. Representative XPS S 2p spectra for PEDOT:PSS-based thermoelectric films: (a) sample A, (b) sample B, (c) sample C, (d) sample D, and (e) sample E. (f) The PSS to PEDOT ratio of sample A-E calculated from XPS S 2p band intensity ratio.

formation of the more oriented PEDOT crystals. To the best of our knowledge, the obtained thermoelectric performance is superior to those of other spray-coated polymer thermoelectric films [44,57–61], primarily due to the highest electrical conductivity, with a more than two-times higher power factor than previously reported.

The temperature-dependent thermoelectric properties of the optimized film (sample D) in the low-temperature range of 303–333 K are presented in Fig. S5. Here, the conductivity of sample D is seen to decrease steadily with increasing temperature, thereby indicating typical metallic behavior [62–64], along with a high carrier density. Meanwhile, the temperature-dependent Seebeck coefficient exhibits the opposite trend, gradually increasing to a maximum of 127.8 μW K^{-2} m^{-1} at 333 K.

2.7. Flexible thermoelectric generator

This high power factor makes the post-treated PEDOT:PSS film a promising building block for demonstrating a proof-of-concept flexible thermoelectric generator. To this end, the spray-printed PEDOT:PSS legs for the generators were fabricated on a PET substrate by masking the desired areas. The PEDOT:PSS legs were interconnected by Ag via thermal evaporation, while the endpoints of the module were connected to the external Ag paste. As shown in Fig. 8a and the inset to Fig. 8c, the final module consisted of 14 legs with lateral dimensions of 2 mm × 15 mm, printed directly onto a 100 mm × 25 mm substrate. The thermoelectric generator was investigated by heating one side with a hot stage while maintaining the other side at ambient temperature. The temperature difference (△T) across the two sides was monitored by external thermocouples that were assembled in contact with the module. The results in Fig. 8b indicate that the voltage-current characteristics are linear under the various △T values of 3.9, 7.2, 10.4, 13.4, 16.6, and 19.5 K, with a maximum output power density of 12.1 nW cm^{-2} at △T = 19.5 K. Thus, the as-fabricated PEDOT:PSS hybrid films are superior to other spray-coated PEDOT:PSS-based thermoelectric generators [44, 65–70] (Fig. 8d), and are potentially applicable as wearable thermoelectric devices under a small temperature gradient by the sustainable conversion of human body heat to electricity.

The mechanical flexibility of the as-fabricated PEDOT:PSS-based thermoelectric generator is demonstrated by measuring the relative changes in output voltage and power density during the controlled bending test in Fig. 8c. Here, no significant change in device performance (<10%) is observed when the thermoelectric module is repeatedly bent to the low bending radius of 20 mm for 1000 cycles. Meanwhile, the environmental stability of the thermoelectric generator is demonstrated in Fig. S6, where the unencapsulated device maintains over 90% of the initial output voltage, and 80% of the initial power density, after 21 days of storage under ambient air with 35–60% relative humidity at room temperature. It should be noted slight decrease in the first five days may be due to the high-humidity environment. These results demonstrate that the as-fabricated PEDOT:PSS is relatively stable without any degradation.

3. Conclusion

The thermoelectric properties of spray-coated PEDOT:PSS films were investigated herein according to the selective removal of excess insulating PSS chains and the enhancement in film morphology via a two-step post-treatment process. Thus, a simultaneous enhancement in both conductivity and Seebeck coefficient was achieved via the treatment with polar EG solvent followed by treatment with the optimal concentration of MAI in DMSO/DI water. In detail, a remarkably high conductivity of 2226.8 S cm^{-1} and a moderately high Seekbeck coefficient of 22.8 mV K^{-1}, giving a maximum power factor of 122.3 μW mK^{-2}, were obtained at 323 K via the use of 0.05 M MAI solution in the second post-treatment step. The doping levels, microstructural/morphological properties, and molecular organization of the as-fabricated PEDOT:PSS films were systematically investigated. In addition, the mechanical flexibility of the spray-coated PEDOT:PSS film was demonstrated, and the film was successfully integrated into an array of fourteen p-type legs directly fabricated on a PET substrate. The resulting flexible thermoelectric generator produced a maximum power density of 12.1 nW cm^{-2} at a temperature gradient of 19.5 K. The results demonstrate the spray deposition of PEDOT:PSS films with a high power factors and good electrical conductivities via the two-step post-treatment process with a polar solvent and salt solution as a viable and facile procedure for the printing of flexible thermoelectric generators.

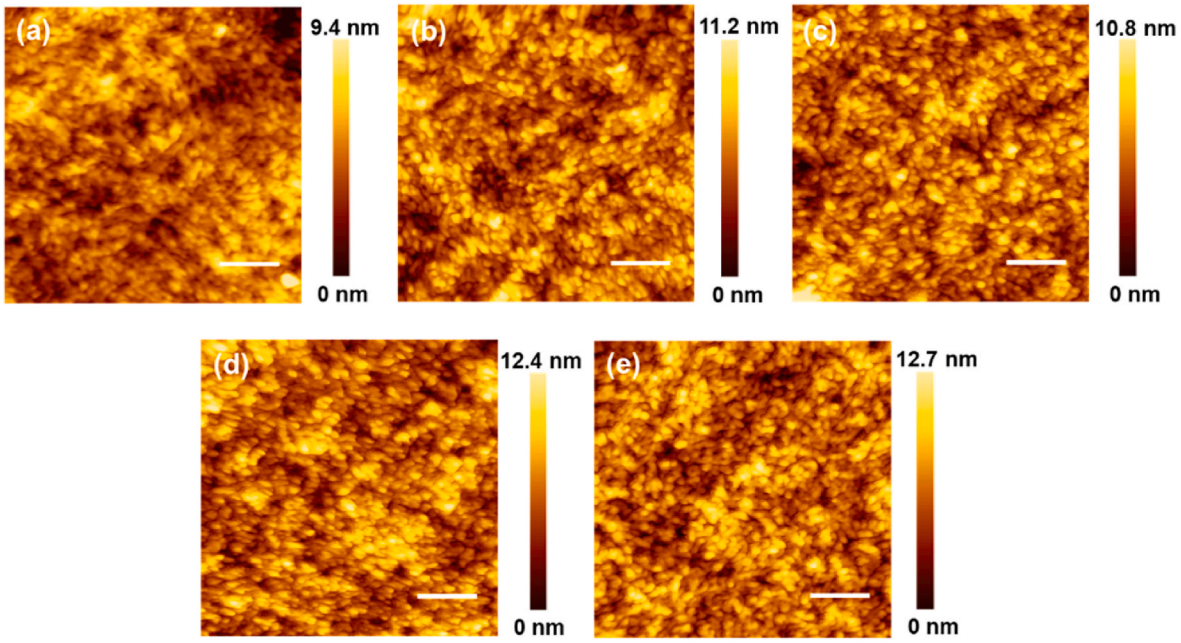

Fig. 3. AFM topographical images of PEDOT:PSS-based thermoelectric films: (a) sample A, (b) sample B, (c) sample C, (d) sample D, and (e) sample E. (scale bar: 200 nm).

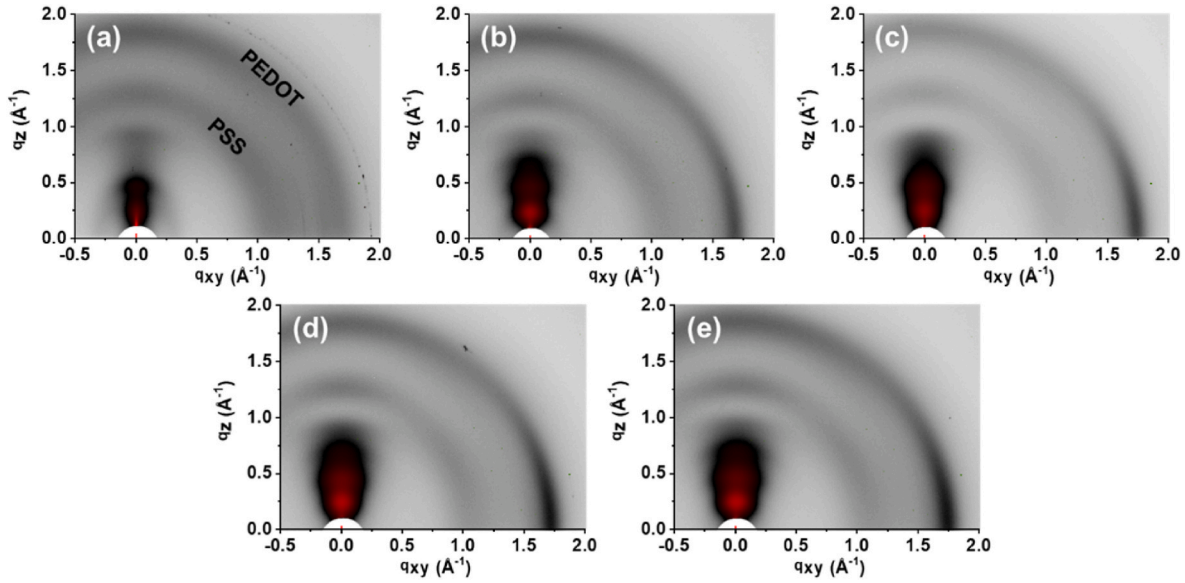

Fig. 4. Two-dimensional GIWAXS patterns of PEDOT:PSS-based thermoelectric films: (a) sample A, (b) sample B, (c) sample C, (d) sample D, and (e) sample E.

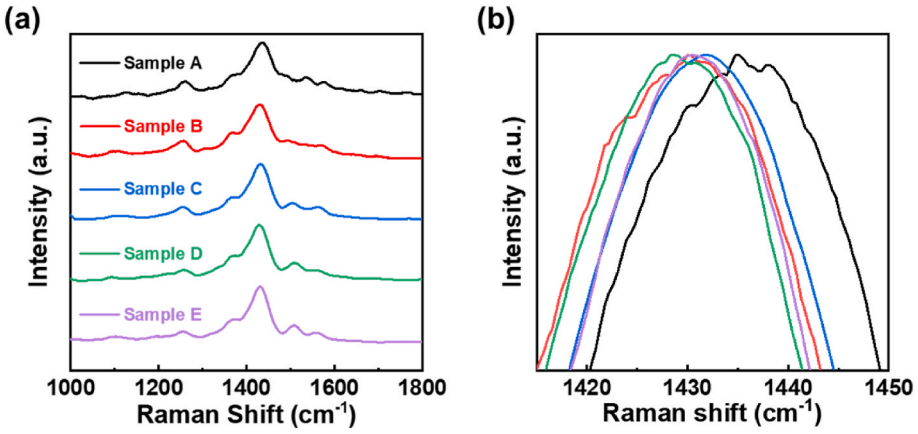

Fig. 5. (a) Raman spectra of PEDOT:PSS-based thermoelectric films (sample A-E). (b) The zoom-in spectra for Raman peak with wavelengths ranging from 1415 to 1450 cm^{-1}.

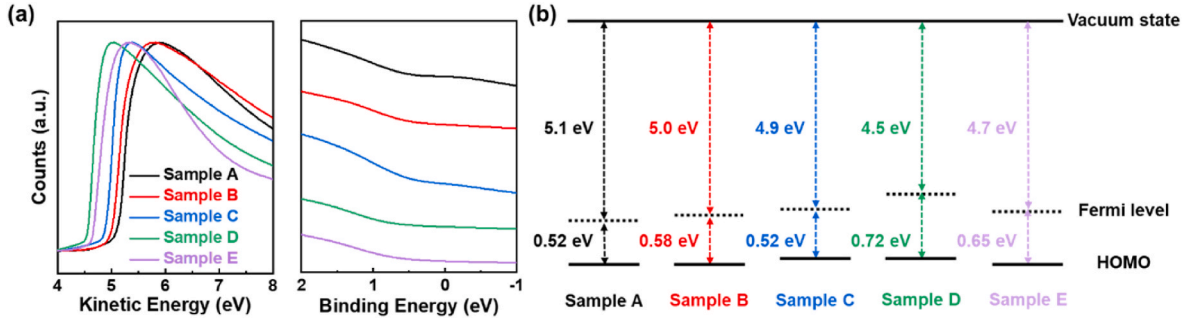

Fig. 6. UPS spectra of (a) secondary electron cutoff region and (b) valence band region near the Fermi level for PEDOT:PSS-based thermoelectric films (sample A-E). (c) Energy level diagram for the sample A-E according to the low level energy and near Fermi level energy region of UPS spectra.

4. Experimental details

4.1. Materials

The PEDOT:PSS aqueous solution (Clevios PH 1000) with concentration of 1.3 wt% and PEDOT:PSS weight ratio of 1:2.5 was purchased from Heraeus and stored in refrigerator. EG was supplied by Alfa Aesar, while DMSO and MAI were received from Sigma-Aldrich, and all were used as received.

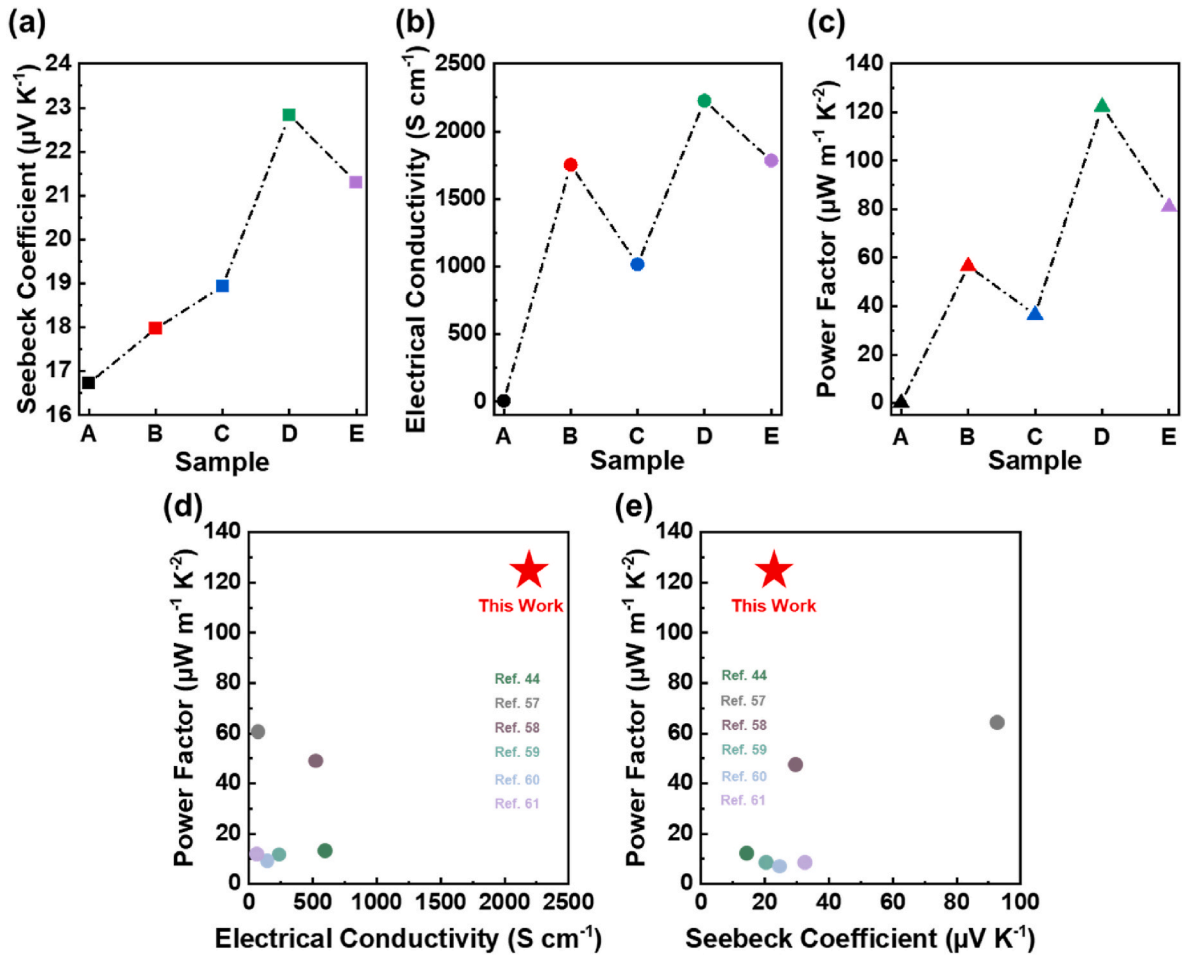

Fig. 7. (a) Seebeck coefficient, (b) electrical conductivity, and (c) power factor for PEDOT:PSS-based thermoelectric films (sample A-E). Comparison of (d) power factor vs. conductivity and (e) power factor vs. conductivity between spray-coated polymer thermoelectric films in this work with values from relevant studies reported in the literature.

4.2. Thermoelectric film fabrication and measurement

The fabrication procedure for modified PEDOT:PSS thermoelectric film is schematically illustrated in Fig. 1. Before spray deposition of the PEDOT:PSS film, the glass substrates were pre-cleaned (in the order of DI water, acetone, and isopropyl alcohol for each 10 min) and UV/ozone-treated for 10 min. The automatic spray-coating nozzle (Lumina LRK-AS8) for injection of solution using compressed air-assist atomization at a pressure of 0.2 MPa was applied. The distance of the nozzle tip to substrates and substrate temperature were fixed at 14 cm, and 80 °C, respectively. The PEDOT:PSS solution was sprayed twice over the substrate with a size of 1.5 × 1.5 cm^2, where each spraying period is controlled to be 2 s, and the interval between two sprayings is around 30 s. After additional annealing at 100 °C for 10 min to obtain the pristine PEDOT:PSS film (sample A), a two-step post-treatment was conducted. EG organic solvent (180 μl dropping) employed to initiate the post-treatment on PEDOT:PSS film was dropped on the PEDOT:PSS surface and transferred to a hot plate (80 °C for 10 min), followed by washing with deionized water three times and drying at 100 °C for 10 min to obtain EG post-treated PEDOT:PSS film (sample B). After that, subsequent MAI post-treatment was performed when dropping 180 μl solution (0.01, 0.05, and 0.1 M MAI in DMSO/DI water (7/3 vol) mixing solvent) onto EG post-treated PEDOT:PSS film and drying under the same condition to obtain the modified PEDOT:PSS films (sample C, D, and E, respectively) with complete post-treatment procedure. The Seebeck coefficient and electrical conductivity were simultaneously measured using commercial ZEM-3 (ADVANCE RIKO Inc., Japan) instrument under 323 K.

4.3. Fabrication and characterization of thermoelectric generator

To fabricate the thermoelectric generators, 14 thermoelectric legs (2 × 15 mm^2) were spray-printed using the PEDOT:PSS solutions through the shadow mask (Fig. 8a) onto the clean PET substrate. The spray-printing/annealing parameters and two-step post-treatment process are all the same as the optimized condition (sample D), except for the moving speed of the spray nozzle at 6.8 cm s^{-1} and six repeated spraying times. For connection of the thermoelectric legs, the series circuit was constructed by thermal evaporation of Ag electrode with a width of 2 mm and a thickness of 100 nm through the second mask. The measurement setup consists of two Peltier units to maintain the separated stages, which can independently function as the hot and cold parts. The temperatures at both ends (painted with Ag paste) of the thermoelectric generators were detected with two thermocouples. A Keithley 2400 source meter, a Keithley 2182A nanovoltmeter, and a Keithley DAQ6510 data acquisition/logging multimeter system was used for the measurements.

CRediT authorship contribution statement

Yen-Ting Lin: Conceptualization, Formal analysis, Investigation, Resources, Writing – original draft, Writing – review & editing, Visualization. **Chia-Yu Lee:** Conceptualization, Formal analysis, Investigation. **Chih-Yao Wu:** Conceptualization, Formal analysis, Investigation. **Jhih-**

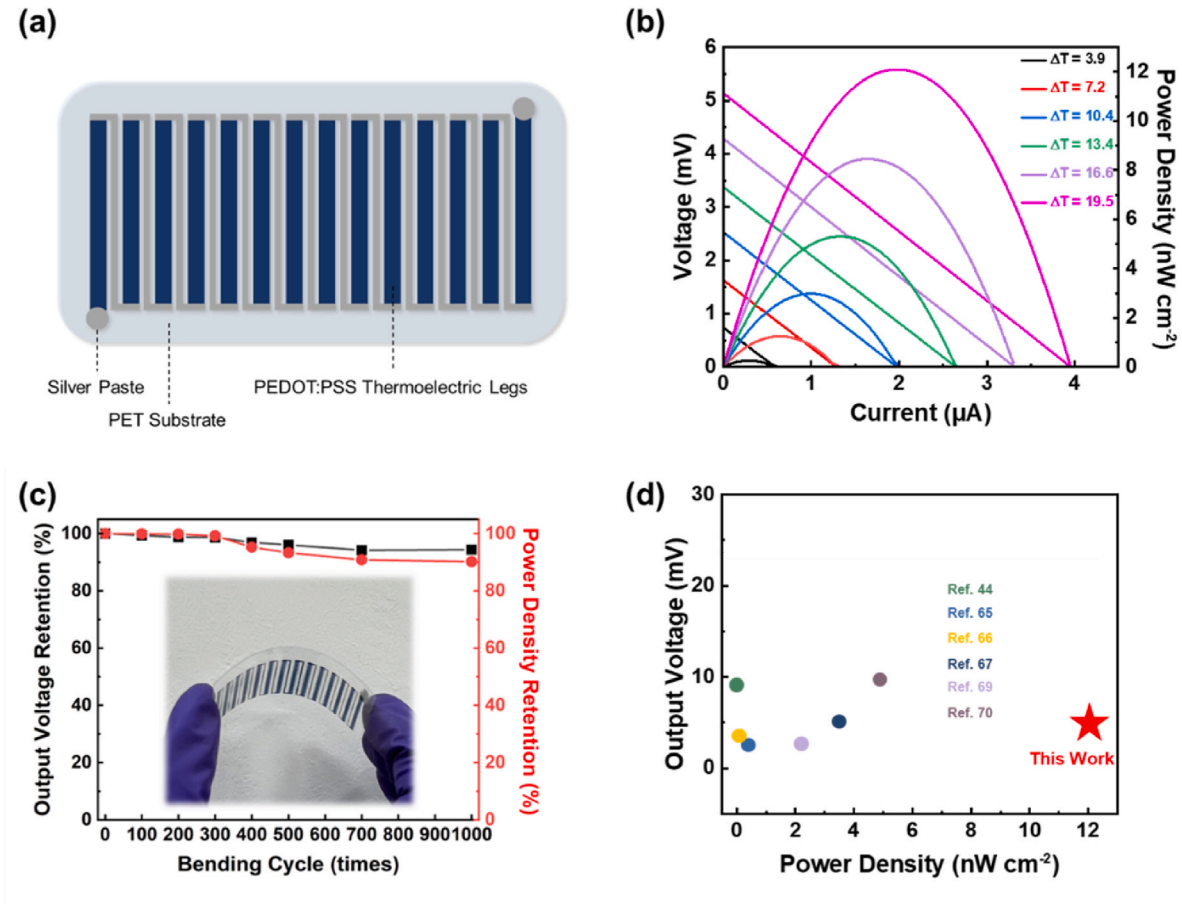

Fig. 8. Thermoelectric performance of thermoelectric generators fabricated from modified PEDOT:PSS film (same fabrication procedure from sample D): (a) Schematic describing planar thermoelectric generators architecture consisting of 14 legs. (b) Output voltage vs. current (filled symbols) and power density vs. current (empty symbols) depending on the temperature gradients. (c) Relative output voltage and relative power density over repeated bending cycles. The insert shows the photograph depicting the bendable thermoelectric generators. (d) Comparison of output voltage vs. power density between the spray-coated PEDOT:PSS-based thermoelectric generators in this work with values from relevant studies reported in the literature.

Min Lin: Conceptualization, Project administration. **Tai-Chou Lee:** Conceptualization, Project administration. **Shih-Huang Tung:** Conceptualization, Writing – original draft, Writing – review & editing. **Cheng-Liang Liu:** Conceptualization, Project administration, Writing – review & editing, Supervision, Funding acquisition.

Declaration of competing interest

The authors declare the following financial interests/personal relationships which may be considered as potential competing interests: Cheng-Liang Liu reports financial support was provided by National Science and Technology Council.

Data availability

Data will be made available on request.

Acknowledgement

The authors acknowledge the financial support from 2030 Cross-Generation Young Scholars Program by the National Science and Technology Council (NSTC) in Taiwan, under grant 111-2628-E-002-014. The authors also thank Beamline TPS 25A at National Synchrotron Radiation Research Center (NSRRC) of Taiwan for providing beamtime.

Appendix A. Supplementary data

Supplementary data to this article can be found online at https://doi.org/10.1016/j.jpowsour.2022.232516.

References

[1] Z. Fan, J. Ouyang, Thermoelectric properties of pedot:Pss, Adv. Electron. Mater. 5 (2019), 1800769, https://doi.org/10.1002/aelm.201800769.
[2] D. Ju, D. Kim, H. Yook, J.W. Han, K. Cho, Controlling electrostatic interaction in pedot:Pss to overcome thermoelectric tradeoff relation, Adv. Funct. Mater. 29 (2019), 1905590, https://doi.org/10.1002/adfm.201905590.
[3] M. Li, Z. Bai, X. Chen, C.-C. Liu, J.-K. Xu, X.-Q. Lan, F.-X. Jiang, Thermoelectric transport in conductive poly(3,4-ethylenedioxythiophene), Chin. Phys. B 31 (2022), 027201, https://doi.org/10.1088/1674-1056/ac4230.
[4] Q. Li, M. Deng, S. Zhang, D. Zhao, Q. Jiang, C. Guo, Q. Zhou, W. Liu, Synergistic enhancement of thermoelectric and mechanical performances of ionic liquid litfsi modulated pedot flexible films, J. Mater. Chem. C 7 (2019) 4374–4381, https://doi.org/10.1039/c9tc00310j.
[5] Q. Li, Q. Zhou, W. Xu, L. Wen, J. Li, B. Deng, J. Zhang, H. Xu, W. Liu, Anion size effect of ionic liquids in tuning the thermoelectric and mechanical properties of pedot:Pss films through a counterion exchange strategy, ACS Appl. Mater. Interfaces 14 (2022) 27911–27921, https://doi.org/10.1021/acsami.2c05591.
[6] I. Petsagkourakis, N. Kim, K. Tybrandt, I. Zozoulenko, X. Crispin, Poly(3,4-ethylenedioxythiophene): chemical synthesis, transport properties, and thermoelectric devices, Adv. Electron. Mater. 5 (2019), 1800918, https://doi.org/10.1002/aelm.201800918.
[7] S. Xu, M. Hong, X. Shi, M. Li, Q. Sun, Q. Chen, M. Dargusch, J. Zou, Z.-G. Chen, Computation-guided design of high-performance flexible thermoelectric modules for sunlight-to-electricity conversion, Energy Environ. Sci. 13 (2020) 3480–3488, https://doi.org/10.1039/d0ee01895c.

[8] Y. Yang, H. Deng, Q. Fu, Recent progress on pedot:Pss based polymer blends and composites for flexible electronics and thermoelectric devices, Mater. Chem. Front. 4 (2020) 3130–3152, https://doi.org/10.1039/d0qm00308e.

[9] J.S. Yun, S. Choi, S.H. Im, Advances in carbon-based thermoelectric materials for high-performance, flexible thermoelectric devices, Carbon Energy 3 (2021) 667–708, https://doi.org/10.1002/cey2.121.

[10] Y. Zheng, H. Zeng, Q. Zhu, J. Xu, Recent advances in conducting poly(3,4-ethylenedioxythiophene):Polystyrene sulfonate hybrids for thermoelectric applications, J. Mater. Chem. C 6 (2018) 8858–8873, https://doi.org/10.1039/c8tc01900b.

[11] Y. Jia, Q. Jiang, H. Sun, P. Liu, D. Hu, Y. Pei, W. Liu, X. Crispin, S. Fabiano, Y. Ma, Y. Cao, Wearable thermoelectric materials and devices for self-powered electronic systems, Adv. Mater. 33 (2021), 2102990, https://doi.org/10.1002/adma.202102990.

[12] S. Wang, G. Zuo, J. Kim, H. Sirringhaus, Progress of conjugated polymers as emerging thermoelectric materials, Prog. Polym. Sci. 129 (2022), 101548, https://doi.org/10.1016/j.progpolymsci.2022.101548.

[13] H. Yao, Z. Fan, P. Li, B. Li, X. Guan, D. Du, J. Ouyang, Solution processed intrinsically conductive polymer films with high thermoelectric properties and good air stability, J. Mater. Chem. 6 (2018) 24496–24502, https://doi.org/10.1039/c8ta08682f.

[14] W. Zhao, J. Ding, Y. Zou, C.A. Di, D. Zhu, Chemical doping of organic semiconductors for thermoelectric applications, Chem. Soc. Rev. 49 (2020) 7210–7228, https://doi.org/10.1039/d0cs00204f.

[15] L. Deng, G. Chen, Recent progress in tuning polymer oriented microstructures for enhanced thermoelectric performance, Nano Energy 80 (2021), 105448, https://doi.org/10.1016/j.nanoen.2020.105448.

[16] Y. Du, J. Xu, B. Paul, P. Eklund, Flexible thermoelectric materials and devices, Appl. Mater. Today 12 (2018) 366–388, https://doi.org/10.1016/j.apmt.2018.07.004.

[17] Y. Lu, J.Y. Wang, J. Pei, Achieving efficient n-doping of conjugated polymers by molecular dopants, Acc. Chem. Res. 54 (2021) 2871–2883, https://doi.org/10.1021/acs.accounts.1c00223.

[18] S. Masoumi, S. O'Shaughnessy, A. Pakdel, Organic-based flexible thermoelectric generators: from materials to devices, Nano Energy 92 (2022), 106774, https://doi.org/10.1016/j.nanoen.2021.106774.

[19] G. Prunet, F. Pawula, G. Fleury, E. Cloutet, A.J. Robinson, G. Hadziioannou, A. Pakdel, A review on conductive polymers and their hybrids for flexible and wearable thermoelectric applications, Mater. Today Phys. 18 (2021), 100402, https://doi.org/10.1016/j.mtphys.2021.100402.

[20] Y. Wang, L. Yang, X.L. Shi, X. Shi, L. Chen, M.S. Dargusch, J. Zou, Z.G. Chen, Flexible thermoelectric materials and generators: challenges and innovations, Adv. Mater. 31 (2019), 1807916, https://doi.org/10.1002/adma.201807916.

[21] L. Bießmann, N. Saxena, N. Hohn, M.A. Hossain, J.G.C. Veinot, P. Müller-Buschbaum, Highly conducting, transparent pedot:Pss polymer electrodes from post-treatment with weak and strong acids, Adv. Electron. Mater. 5 (2019), 1800654, https://doi.org/10.1002/aelm.201800654.

[22] Z. Fan, D. Du, H. Yao, J. Ouyang, Higher pedot molecular weight giving rise to higher thermoelectric property of pedot:Pss: a comparative study of clevios p and clevios ph1000, ACS Appl. Mater. Interfaces 9 (2017) 11732–11738, https://doi.org/10.1021/acsami.6b15158.

[23] J. Luo, D. Billep, T. Waechtler, T. Otto, M. Toader, O. Gordan, E. Sheremet, J. Martin, M. Hietschold, D.R.T. Zahn, T. Gessner, Enhancement of the thermoelectric properties of pedot:Pss thin films by post-treatment, J. Mater. Chem. 1 (2013) 7576–7583, https://doi.org/10.1039/c3ta11209h.

[24] A.L. Oechsle, J.E. Heger, N. Li, S. Yin, S. Bernstorff, P. Muller-Buschbaum, In situ observation of morphological and oxidation level degradation processes within ionic liquid post-treated pedot:Pss thin films upon operation at high temperatures, ACS Appl. Mater. Interfaces 14 (2022) 30802–30811, https://doi.org/10.1021/acsami.2c05745.

[25] N. Saxena, B. Pretzl, X. Lamprecht, L. Biessmann, D. Yang, N. Li, C. Bilko, S. Bernstorff, P. Muller-Buschbaum, Ionic liquids as post-treatment agents for simultaneous improvement of seebeck coefficient and electrical conductivity in pedot:Pss films, ACS Appl. Mater. Interfaces 11 (2019) 8060–8071, https://doi.org/10.1021/acsami.8b21709.

[26] X. Wang, A.K.K. Kyaw, C. Yin, F. Wang, Q. Zhu, T. Tang, P.I. Yee, J. Xu, Enhancement of thermoelectric performance of pedot:Pss films by post-treatment with a superacid, RSC Adv. 8 (2018) 18334–18340, https://doi.org/10.1039/c8ra02058b.

[27] J. Liu, Y. Jia, Q. Jiang, F. Jiang, C. Li, X. Wang, P. Liu, P. Liu, F. Hu, Y. Du, J. Xu, Highly conductive hydrogel polymer fibers toward promising wearable thermoelectric energy harvesting, ACS Appl. Mater. Interfaces 10 (2018) 44033–44040, https://doi.org/10.1021/acsami.8b15332.

[28] W. Lee, Y.H. Kang, J.Y. Lee, K.-S. Jang, S.Y. Cho, Improving the thermoelectric power factor of cnt/pedot:Pss nanocomposite films by ethylene glycol treatment, RSC Adv. 6 (2016) 53339–53344, https://doi.org/10.1039/c6ra08599g.

[29] X. Huang, L. Deng, F. Liu, Z. Liu, G. Chen, Aggregate structure evolution induced by annealing and subsequent solvent post-treatment for thermoelectric property enhancement of pedot:Pss films, J. Chem. Eng. 417 (2021), 129230, https://doi.org/10.1016/j.cej.2021.129230.

[30] J. Luo, D. Billep, T. Blaudeck, E. Sheremet, R.D. Rodriguez, D.R.T. Zahn, M. Toader, M. Hietschold, T. Otto, T. Gessner, Chemical post-treatment and thermoelectric properties of poly(3,4-ethylenedioxylthiophene):Poly (styrenesulfonate) thin films, J. Appl. Phys. 115 (2014), 054908, https://doi.org/10.1063/1.4864749.

[31] A.C. Hinckley, S.C. Andrews, M.T. Dunham, A. Sood, M.T. Barako, S. Schneider, M. F. Toney, K.E. Goodson, Z. Bao, Achieving high thermoelectric performance and metallic transport in solvent-sheared pedot:Pss, Adv. Electron. Mater. 7 (2021), 2001190, https://doi.org/10.1002/aelm.202001190.

[32] S. Zhang, Z. Fan, X. Wang, Z. Zhang, J. Ouyang, Enhancement of the thermoelectric properties of pedot:Pss via one-step treatment with cosolvents or their solutions of organic salts, J. Mater. Chem. 6 (2018) 7080–7087, https://doi.org/10.1039/c7ta11148g.

[33] Z. Fan, P. Li, D. Du, J. Ouyang, Significantly enhanced thermoelectric properties of pedot:Pss films through sequential post-treatments with common acids and bases, Adv. Energy Mater. 7 (2017), 1602116, https://doi.org/10.1002/aenm.201602116.

[34] A.K.K. Kyaw, T.A. Yemata, X. Wang, S.L. Lim, W.S. Chin, K. Hippalgaonkar, J. Xu, Enhanced thermoelectric performance of pedot:Pss films by sequential post-treatment with formamide, Macromol. Mater. Eng. 303 (2018), 1700429, https://doi.org/10.1002/mame.201700429.

[35] S.H. Lee, H. Park, S. Kim, W. Son, I.W. Cheong, J.H. Kim, Transparent and flexible organic semiconductor nanofilms with enhanced thermoelectric efficiency, J. Mater. Chem. 2 (2014) 7288–7294, https://doi.org/10.1039/c4ta00700j.

[36] X. Li, C. Liu, W. Zhou, X. Duan, Y. Du, J. Xu, C. Li, J. Liu, Y. Jia, P. Liu, Q. Jiang, C. Luo, C. Liu, F. Jiang, Roles of polyethylenimine ethoxylated in efficiently tuning the thermoelectric performance of poly(3,4-ethylenedioxythiophene)-rich nanocrystal films, ACS Appl. Mater. Interfaces 11 (2019) 8138–8147, https://doi.org/10.1021/acsami.9b00298.

[37] H. Park, S.H. Lee, F.S. Kim, H.H. Choi, I.W. Cheong, J.H. Kim, Enhanced thermoelectric properties of pedot:Pss nanofilms by a chemical dedoping process, J. Mater. Chem. 2 (2014) 6532–6539, https://doi.org/10.1039/c3ta14960a.

[38] S. Tu, T. Tian, A. Lena Oechsle, S. Yin, X. Jiang, W. Cao, N. Li, M.A. Scheel, L. K. Reb, S. Hou, A.S. Bandarenka, M. Schwartzkopf, S.V. Roth, P. Müller-Buschbaum, Improvement of the thermoelectric properties of pedot:Pss films via dmso addition and dmso/salt post-treatment resolved from a fundamental view, J. Chem. Eng. 429 (2022), 132295, https://doi.org/10.1016/j.cej.2021.132295.

[39] C. Wang, K. Sun, J. Fu, R. Chen, M. Li, Z. Zang, X. Liu, B. Li, H. Gong, J. Ouyang, Enhancement of conductivity and thermoelectric property of pedot:Pss via acid doping and single post-treatment for flexible power generator, Adv. Sustain. Syst. 2 (2018), 1800085, https://doi.org/10.1002/adsu.201800085.

[40] S. Xu, M. Hong, X.-L. Shi, Y. Wang, L. Ge, Y. Bai, L. Wang, M. Dargusch, J. Zou, Z.-G. Chen, High-performance pedot:Pss flexible thermoelectric materials and their devices by triple post-treatments, Chem. Mater. 31 (2019) 5238–5244, https://doi.org/10.1021/acs.chemmater.9b01500.

[41] M. Zeng, D. Zavanelli, J. Chen, M. Saeidi-Javash, Y. Du, S. LeBlanc, G.J. Snyder, Y. Zhang, Printing thermoelectric inks toward next-generation energy and thermal devices, Chem. Soc. Rev. 51 (2022) 485–512, https://doi.org/10.1039/d1cs00490e.

[42] E.J. Bae, Y.H. Kang, C. Lee, S.Y. Cho, Engineered nanocarbon mixing for enhancing the thermoelectric properties of a telluride-pedot:Pss nanocomposite, J. Mater. Chem. 5 (2017) 17867–17873, https://doi.org/10.1039/c7ta04280a.

[43] C.T. Hong, Y.H. Kang, J. Ryu, S.Y. Cho, K.-S. Jang, Spray-printed cnt/p3ht organic thermoelectric films and power generators, J. Mater. Chem. 3 (2015) 21428–21433, https://doi.org/10.1039/c5ta06096f.

[44] S. Hwang, I. Jeong, J. Park, J.K. Kim, H. Kim, T. Lee, J. Kwak, S. Chung, Enhanced output performance of all-solution-processed organic thermoelectrics: spray printing and interface engineering, ACS Appl. Mater. Interfaces 12 (2020) 26250–26257, https://doi.org/10.1021/acsami.0c04550.

[45] E. Yvenou, M. Sandroni, A. Carella, M.N. Gueye, J. Faure-Vincent, S. Pouget, R. Demadrille, J.-P. Simonato, Spray-coated pedot:Otf films: thermoelectric properties and integration into a printed thermoelectric generator, Mater. Chem. Front. 4 (2020) 2054–2063, https://doi.org/10.1039/d0qm00265h.

[46] D. Alemu, H.-Y. Wei, K.-C. Ho, C.-W. Chu, Highly conductive pedot:Pss electrode by simple film treatment with methanol for ito-free polymer solar cells, Energy Environ. Sci. 5 (2012) 9662–9671, https://doi.org/10.1039/c2ee22595f.

[47] J. Dong, G. Portale, Role of the processing solvent on the electrical conductivity of pedot:Pss, Adv. Mater. Interfac. 7 (2020), 2000641, https://doi.org/10.1002/admi.202000641.

[48] H. Lee, E. Puodziukynaite, Y. Zhang, J.C. Stephenson, L.J. Richter, D.A. Fischer, D. M. DeLongchamp, T. Emrick, A.L. Briseno, Poly(sulfobetaine methacrylate)s as electrode modifiers for inverted organic electronics, J. Am. Chem. Soc. 137 (2015) 540–549, https://doi.org/10.1021/ja512148d.

[49] M.R. Lenze, N.M. Kronenberg, F. Würthner, K. Meerholz, In-situ modification of pedot:Pss work function using alkyl alcohols as secondary processing solvents and their impact on merocyanine based bulk heterojunction solar cells, Org. Electron. 21 (2015) 171–176, https://doi.org/10.1016/j.orgel.2015.03.008.

[50] D.J. Yun, J. Jung, Y.M. Sung, H. Ra, J.M. Kim, J. Chung, S.Y. Kim, Y.S. Kim, S. Heo, K.H. Kim, Y.J. Jeong, J. Jang, In-situ photoelectron spectroscopy study on the air degradation of pedot:Pss in terms of electrical and thermoelectric properties, Adv. Electron. Mater. 6 (2020), 2000620, https://doi.org/10.1002/aelm.202000620.

[51] O. Bubnova, Z.U. Khan, H. Wang, S. Braun, D.R. Evans, M. Fabretto, P. Hojati-Talemi, D. Dagnelund, J.B. Arlin, Y.H. Geerts, S. Desbief, D.W. Breiby, J. W. Andreasen, R. Lazzaroni, W.M. Chen, I. Zozoulenko, M. Fahlman, P.J. Murphy, M. Berggren, X. Crispin, Semi-metallic polymers, Nat. Mater. 13 (2014) 190–194, https://doi.org/10.1038/nmat3824.

[52] K. Jiang, S.-H. Hong, S.-H. Tung, C.-L. Liu, Effects of cation size on thermoelectricity of pedot:Pss/ionic liquid hybrid films for wearable thermoelectric generator application, J. Mater. Chem. 10 (2022) 18792–18802, https://doi.org/10.1039/d2ta05134f.

[53] S.S. Kalagi, P.S. Patil, Secondary electrochemical doping level effects on polaron and bipolaron bands evolution and interband transition energy from absorbance spectra of pedot: pss thin films, Synth. Met. 220 (2016) 661–666, https://doi.org/10.1016/j.synthmet.2016.08.009.
[54] J. Ouyang, Q. Xu, C.-W. Chu, Y. Yang, G. Li, J. Shinar, On the mechanism of conductivity enhancement in poly(3,4-ethylenedioxythiophene):Poly(styrene sulfonate) film through solvent treatment, Polymer 45 (2004) 8443–8450, https://doi.org/10.1016/j.polymer.2004.10.001.
[55] H. Fritzsche, A general expression for the thermoelectric power, Solid State Commun. 9 (1971) 1813–1815.
[56] J.M. Buhmann, M. Sigrist, Thermoelectric effect of correlated metals: band-structure effects and the breakdown of mott's formula, Phys. Rev. B 88 (2013), 115128, https://doi.org/10.1103/PhysRevB.88.115128.
[57] E.J. Bae, Y.H. Kang, K.S. Jang, C. Lee, S.Y. Cho, Solution synthesis of telluride-based nano-barbell structures coated with pedot:Pss for spray-printed thermoelectric generators, Nanoscale 8 (2016) 10885–10890, https://doi.org/10.1039/c5nr07032e.
[58] R. Sarabia-Riquelme, G. Ramos-Fernández, I. Martin-Gullon, M.C. Weisenberger, Synergistic effect of graphene oxide and wet-chemical hydrazine/deionized water solution treatment on the thermoelectric properties of pedot:Pss sprayed films, Synth. Met. 222 (2016) 330–337, https://doi.org/10.1016/j.synthmet.2016.11.013.
[59] J.F. Ponder, A.K. Menon, R.R. Dasari, S.L. Pittelli, K.J. Thorley, S.K. Yee, S. R. Marder, J.R. Reynolds, Conductive, solution-processed dioxythiophene copolymers for thermoelectric and transparent electrode applications, Adv. Energy Mater. 9 (2019), 1900395, https://doi.org/10.1002/aenm.201900395.
[60] L. Shen, P. Liu, C. Liu, Q. Jiang, J. Xu, X. Duan, Y. Du, F. Jiang, Advances in efficient polymerization of solid-state trithiophenes for organic thermoelectric thin-film, ACS Appl. Polym. Mater. 2 (2019) 376–384, https://doi.org/10.1021/acsapm.9b00842.
[61] S. Mardi, P. Cataldi, A. Athanassiou, A. Reale, 3d cellulose fiber networks modified by pedot:Pss/graphene nanoplatelets for thermoelectric applications, Appl. Phys. Lett. 120 (2022), 033102, https://doi.org/10.1063/5.0075918.
[62] N. Massonnet, A. Carella, A. de Geyer, J. Faure-Vincent, J.P. Simonato, Metallic behaviour of acid doped highly conductive polymers, Chem. Sci. 6 (2015) 412–417, https://doi.org/10.1039/c4sc02463j.
[63] P. Stadler, D. Farka, H. Coskun, E.D. Głowacki, C. Yumusak, L.M. Uiberlacker, S. Hild, L.N. Leonat, M.C. Scharber, P. Klapetek, R. Menon, N.S. Sariciftci, Local order drives the metallic state in pedot:Pss, J. Mater. Chem. C 4 (2016) 6982–6987, https://doi.org/10.1039/c6tc02129h.
[64] Z. Yu, Y. Xia, D. Du, J. Ouyang, Pedot:Pss films with metallic conductivity through a treatment with common organic solutions of organic salts and their application as a transparent electrode of polymer solar cells, ACS Appl. Mater. Interfaces 8 (2016) 11629–11638, https://doi.org/10.1021/acsami.6b00317.
[65] L.K. Allison, T.L. Andrew, A wearable all-fabric thermoelectric generator, Adv. Mater. Technol. 4 (2019), 1800615, https://doi.org/10.1002/admt.201800615.
[66] H.M. Elmoughni, A.K. Menon, R.M.W. Wolfe, S.K. Yee, A textile-integrated polymer thermoelectric generator for body heat harvesting, Adv. Mater. Technol. 4 (2019), 1800708, https://doi.org/10.1002/admt.201800708.
[67] Y. Jia, L. Shen, J. Liu, W. Zhou, Y. Du, J. Xu, C. Liu, G. Zhang, Z. Zhang, F. Jiang, An efficient pedot-coated textile for wearable thermoelectric generators and strain sensors, J. Mater. Chem. C 7 (2019) 3496–3502, https://doi.org/10.1039/c8tc05906c.
[68] S. Jin, T. Sun, Y. Fan, L. Wang, M. Zhu, J. Yang, W. Jiang, Synthesis of freestanding pedot:Pss/pva@ag nps nanofiber film for high-performance flexible thermoelectric generator, Polymer 167 (2019) 102–108, https://doi.org/10.1016/j.polymer.2019.01.065.
[69] D. Liu, Z. Yan, Y. Zhao, Z. Zhang, Y. Zhen, B. Zhang, P. Shi, C. Xue, Facile mwcnts-snse/pedot:Pss ternary composite flexible thermoelectric films optimized by cold-pressing, J. Mater. Res. Technol. 15 (2021) 4452–4460, https://doi.org/10.1016/j.jmrt.2021.10.075.
[70] I. Paulraj, T.F. Liang, T.S. Yang, C.H. Wang, J.L. Chen, Y.W. Wang, C.J. Liu, High performance of post-treated pedot:Pss thin films for thermoelectric power generation applications, ACS Appl. Mater. Interfaces 13 (2021) 42977–42990, https://doi.org/10.1021/acsami.1c13968.